

Article

# Nonlinear Excitations in Ultracold Atoms Trapped in Triple Optical Lattices

Pradosh Basu, Barun Halder, Sriganapathy Raghav and Utpal Roy \* 

Department of Physics, Indian Institute of Technology Patna, Patna 801103, India

\* Correspondence: uroy@iitp.ac.in

**Abstract:** Various solitary wave excitations are found for a Bose-Einstein condensate in presence of two hybrid potentials in the form of triple mixtures of optical lattices. One of these potentials comprises of a combination of two important lattice profiles, such as frustrated optical lattice and double-well super-lattice, within one. Another represents a composite lattice combination, resulting in a wider and deeper frustrated optical lattice. The dynamical equation for such a system is solved by the exact analytical method to obtain a bright solitary wave, periodic wave and cnoidal wave excitations. We also report Anderson localization, bifurcation of condensate at the center and a competition between two different types of localizations upon trap engineering. Dynamical and structural stability analyses are also carried out, which reveal the obtained solutions as extremely stable for structural noise incorporation and sufficiently stable for dynamical stability. These triple mixtures of optical lattices impart better tunability on the condensate profile, which has made this system a true quantum simulator.

**Keywords:** solitary waves; triple optical lattices; Bose-Einstein condensate



**Citation:** Basu, P.; Halder, B.; Raghav, S.; Roy, U. Nonlinear Excitations in Ultracold Atoms Trapped in Triple Optical Lattices. *Condens. Matter* **2022**, *7*, 52. <https://doi.org/10.3390/condmat7030052>

Academic Editors: Andrea Perali, Luca Dell'Anna and Luca Salasnich

Received: 4 August 2022

Accepted: 31 August 2022

Published: 9 September 2022

**Publisher's Note:** MDPI stays neutral with regard to jurisdictional claims in published maps and institutional affiliations.



**Copyright:** © 2022 by the authors. Licensee MDPI, Basel, Switzerland. This article is an open access article distributed under the terms and conditions of the Creative Commons Attribution (CC BY) license (<https://creativecommons.org/licenses/by/4.0/>).

## 1. Introduction

Solitary waves are spatially localized, non-decaying waves that retain their shape during propagation. They commonly arise due to the balance between nonlinearity and dispersion in a medium. In 1834, these waves were first observed by John Scott Russell in the Union Canal of Scotland, and these waves are widely studied for various systems such as optical fiber and Bose-Einstein condensate (BEC). The nonlinear Schrödinger equation (NLSE) is well-known to manifest bright and dark solitary waves. To study the solitary waves in a BEC of a dilute quantum gas, the Gross-Pitaevskii equation (GPE) with cubic nonlinearity is commonly used [1–3]. The solution of GPE supports a variety of solitary wave solutions. The bright and the dark solitons arise due to attractive and repulsive interatomic interactions, respectively. The bright soliton represents the propagation of a localized density elevation, whereas the dark soliton represents the propagation of the density depression of the condensate.

BEC, without external confinement, is ideally seen as a highly localized object in momentum space and a delocalized object in position space. However, spatial control can be incorporated, in practice, by engineering external potentials [4], which can reduce the system to lower dimensions and also bring in the possibility of a number of recent technological advancements. To study various applications in BEC, such as quantum simulation, an engineered optical lattice (OL) is of paramount importance. Two or more counter-propagating interfering laser beams (depending upon the dimension of the OL) form a standing wave with an array of crest-trough mixtures. For two constituent lasers, the standing wave is known as an OL for its similarity with the repetitive structure of the crystal lattice [5]. The laser arrangements determine the direction and dimension of the OL. Ultracold atoms are trapped in the troughs of the OL to form the BEC under specific conditions. With the observation of phenomena, such as Anderson-like localization [6,7], negative

absolute temperature [8,9], quantum magnetism [10], quantum droplets [11], and fermionic BEC related to BCS-BEC crossover [12–14], studies related to BEC in OL have become an emerging direction. Recently, this subject has also established its prospects toward applications in precision measurements [15], matter-wave interferometry [16], large-scale magnetic simulators [17], as well as in spin liquids [18,19], quantum simulation [20–22], molecular dynamics [23–25], quantum machine learning [26,27], quantum metrology [28,29], quantum sensing [30,31], quantum communication, and quantum technologies [32–35]. Theoretical studies in this domain are mostly confined to the studies of bichromatic optical lattices (BOLs), with some works in higher-order OLs. On the other hand, the multi-fold OLs provide additional control of atom trapping and allow for more precise measurements, and it also helps in the study of complex solitons [36]. Finding exact solutions for BECs under various confinements is of paramount importance. The exact analytical solutions for BEC are available for potentials, such as harmonic, double-well, periodic, BOL, four-color optical lattice (FOL), triple well, etc. [37–48].

In this work, we aim to find the exact analytical solution for a BEC under triple optical lattice (TOL) of commensurate wavelengths. We introduce two examples of TOL, which can be used to trap a cigar-shaped BEC with cubic nonlinearity. The GPE for such a system is used to find the interrelation between the nonlinear and potential parameters. The exact analytical solution is then obtained for a variety of solitary wave excitations. A triple mixture of OLs imparts better tunability on the condensate profile. The stability of the obtained wavefunctions is also studied and demonstrated by adding random white noise to the wavefunction and also to the external trap.

## 2. Solitary Wave Solution Under the Novel TOL Traps

In this section, we intend to investigate the effects of two different combinations of TOL. An exact analytical model is constructed to discuss the dynamical behavior of 1D BEC and the allowed periods of the TOL combination. The TOL with commensurate wave numbers,  $l$ ,  $2l$ , and  $3l$  should have been the obvious choice. However, it is found that this combination does not support a solitary wave excitation. Therefore, we have considered studying two TOLs with commensurate wavenumbers, (1)  $l$ ,  $3l$ , and  $4l$ , and (2)  $2l$ ,  $3l$  and  $4l$ , and they are labeled as TOL-1 and TOL-2, respectively. Notice that the first lattice is a combination of prime numbered OLs, whereas the second TOL is of the composite type.

TOL-1:

$$V_1(z) = V_{11} \cos(lz) + V_{12} \cos(3lz) + V_{13} \cos(4lz), \tag{1}$$

TOL-2:

$$V_2(z) = V_{21} \cos(2lz) + V_{22} \cos(3lz) + V_{23} \cos(4lz). \tag{2}$$

In Equations (1) and (2), the terms,  $V_{ij}$  ( $j = 1, 2, 3$  for  $i = 1, 2$ ), represent the potential depths. The lattice wave vector  $l$  is related to the recoil energy,  $E_R = \frac{2\pi^2\hbar^2}{M\lambda_l^2}$ , where  $M$  is the mass of the BEC atom, and  $\lambda_l$  is the wavelength of the primary laser. The lattice wave vector, in terms of the oscillator length in the radial direction,  $a_r = (\frac{\hbar}{M\omega_r})^{1/2}$ , is given by,  $l = \frac{2\pi a_r}{\lambda_l}$ , where  $\omega_r$  is the radial frequency. The dimensionless 1D GPE with cubic nonlinearity is given by,

$$\left[ i \frac{\partial}{\partial t} + \frac{1}{2} \frac{\partial^2}{\partial z^2} - g(z, t) |\psi(z, t)|^2 - V(z) - i\zeta(z, t) \right] \psi(z, t) = 0. \tag{3}$$

Here,  $g(z, t)$  and  $\zeta(z, t)$  are the space- and time-modulated terms for nonlinearity and loss/gain of the condensate atoms.  $V(z)$  is the external trapping potential, which will be taken, either TOL-1 or TOL-2. To demonstrate the results, we have considered the experimental parameters for quasi 1D BEC with  $\text{Li}^7$  atoms with an s-wave scattering wavelength of  $a_s = -0.21$  nm, the transverse frequency of the  $\text{CO}_2$  laser  $\omega_r = 2\pi \times 710$  Hz and  $\lambda_l = 10.62$   $\mu\text{m}$  [5]. A direct solution to the above GPE with distributed coefficients is

quite nontrivial, and thus, we use the following similarity transformation, which is known to map it to a known nonlinear equation with constant coefficients [3,49,50]:

$$\psi(z, t) = A(z, t)B[Q(z, t)]e^{i\phi(z, t)}, \tag{4}$$

where  $A(z, t)$ ,  $\phi(z, t)$ ,  $Q(z, t)$ , and  $B[Q(z, t)]$  are the space-time varying amplitude, phase, traveling coordinate, and condensate form factor, respectively. Substituting this ansatz solution into Equation (3) will generate several consistency conditions, which will help us to get the exact solution along with a mapping to the nonlinear differential equation,

$$\frac{\partial^2 B[Q(z, t)]}{\partial Q(z, t)^2} - GB^3[Q(z, t)] = 0, \tag{5}$$

where  $G$  is the nonlinearity constant, which can be controlled by tuning the  $s$ -wave scattering length and can be negative or positive for attractive and repulsive interactions, respectively. Equation (5) is a well-known nonlinear partial differential equation, whose solutions are familiar as 12 Jacobi elliptic functions (three basic functions,  $cn[z, m]$ ,  $sn[z, m]$ , and  $dn[z, m]$ , and their combinations for  $m \in [0, 1]$ , being the modulus parameter) [51]. Therefore, it is evident that one can have a wide range of available solutions depending upon the value of  $m$ . The other consistency conditions, obtained by substituting the similarity transformation of Equation (4) into the GPE, can be written as

$$\begin{aligned} GQ_z^2(z, t) - 2A^2(z, t)g(z, t) &= 0, \\ [A^2(z, t)Q_z(z, t)]_z &= 0, \\ \frac{A_{zz}(z, t)}{2A(z, t)} - \frac{\phi_z^2(z, t)}{2} - \phi_t(z, t) - V(z) &= 0, \\ Q_t(z, t) + Q_z(z, t)\phi_z(z, t) &= 0, \\ 2A(z, t)A_t(z, t) + [A^2(z, t)\phi_z(z, t)]_z - 2\zeta(z, t)A^2(z, t) &= 0. \end{aligned} \tag{6}$$

Here, the subscripts represent the partial differentiation with respect to the corresponding variable. On further simplification, Equation (6) reveals that the coefficient of nonlinearity and the phase are dependent upon the amplitude, whereas the amplitude itself is dependent upon the traveling coordinate.

$$Q(z, t) = \frac{a(t)}{A^2(z, t)}, \quad \phi_z(z, t) = -\frac{A_t(z, t)}{A_z(z, t)}, \tag{7}$$

$$g(z, t) = GQ_z^2(z, t)/2A^2(z, t),$$

where  $a(t)$  is a time-dependent function that arises due to the integration concerning the space coordinate to capture any explicit time dependence of the condensate profile. To find the explicit form of the traveling coordinate, we need to consider the form of the external trapping potential. After substituting the expressions of the potentials from Equations (1) and (2), respectively, we find the expressions for amplitude, phase, loss/gain, and nonlinearity for both the TOLs as,

TOL-1:

$$\begin{aligned}
 A(z, t) &= \sqrt{\frac{a(t)}{\eta \exp\left[\beta_1 \cos(lz) + \frac{\beta_1^2}{16} \cos(2lz)\right]}}, \\
 \phi(z, t) &= \left[1 + \frac{\beta_1^2}{256}\right] \frac{l^2 \beta_1^2}{16} t, \quad \xi(z, t) = \frac{1}{2} \frac{a_t(t)}{a(t)}, \\
 g(z, t) &= \frac{G\eta^4}{2a^2(t)} \exp\left[4\beta_1 \cos(lz) + \frac{\beta_1^2}{4} \cos(2lz)\right],
 \end{aligned} \tag{8}$$

TOL-2:

$$\begin{aligned}
 A(z, t) &= \sqrt{\frac{a(t)}{\eta \exp[\beta_2 \cos(lz) - \cos(2lz)]}}, \\
 \phi(z, t) &= \left[\frac{1 + \beta_2^2}{16}\right] l^2 t, \quad \xi(z, t) = \frac{1}{2} \frac{a_t(t)}{a(t)}, \\
 g(z, t) &= \frac{G\eta^4}{2a^2(t)} \exp[4\beta_2 \cos(lz) - 4 \cos(2lz)].
 \end{aligned} \tag{9}$$

$\beta_1$  and  $\beta_2$  are constants related to the power of the laser beams for TOL-1 and TOL-2, respectively.  $\eta$  represents a dimensionless constant, which is physically related to the width of the condensate profile. The depth of the TOL potentials is determined by  $l$ ,  $\beta_1$  and  $\beta_2$ :

TOL-1:

$$\begin{aligned}
 V_{11} &= \left(1 + \frac{\beta_1^2}{16}\right) \frac{\beta_1 l^2}{4}, \quad V_{12} = -\frac{\beta_1^3 l^2}{64}, \\
 V_{13} &= -\frac{\beta_1^4 l^2}{1024},
 \end{aligned} \tag{10}$$

TOL-2:

$$\begin{aligned}
 V_{21} &= -\left(1 + \frac{\beta_2^2}{16}\right) l^2, \quad V_{22} = \frac{\beta_2 l^2}{4}, \\
 V_{23} &= -\frac{l^2}{4}.
 \end{aligned} \tag{11}$$

From the expression of the above-mentioned laser parameters and the evaluated solution parameters, we can now write down the complete solutions with elliptic function,  $cn$ , for the attractive case ( $G < 0$ ) and with an elliptic function,  $sn$ , for the repulsive case ( $G > 0$ ):

TOL-1:

$$\begin{aligned}
 \psi(z, t) &= \sqrt{\frac{a(t)}{\eta \exp\left[\beta_1 \cos(lz) + \frac{\beta_1^2}{16} \cos(2lz)\right]}} \\
 &\times cn\left[\eta \int_0^z \exp\left[\beta_1 \cos(lz') + \frac{\beta_1^2}{16} \cos(2lz')\right] dz', m\right] \exp[i\phi(z, t)],
 \end{aligned} \tag{12}$$

$$\begin{aligned} \psi(z, t) &= \sqrt{\frac{a(t)}{\eta \exp\left[\beta_1 \cos(lz) + \frac{\beta_1^2}{16} \cos(2lz)\right]}} \\ &\times \operatorname{sn}\left[\eta \int_0^z \exp\left[\beta_1 \cos(lz') + \frac{\beta_1^2}{16} \cos(2lz')\right] dz', m\right] \exp[i\phi(z, t)], \end{aligned} \tag{13}$$

TOL-2:

$$\begin{aligned} \psi(z, t) &= \sqrt{\frac{a(t)}{\eta \exp[\beta_2 \cos(lz) - \cos(2lz)]}} \\ &\times \operatorname{cn}\left[\eta \int_0^z \exp[\beta_2 \cos(lz') - \cos(2lz')] dz', m\right] \exp[i\phi(z, t)], \end{aligned} \tag{14}$$

$$\begin{aligned} \psi(z, t) &= \sqrt{\frac{a(t)}{\eta \exp[\beta_2 \cos(lz) - \cos(2lz)]}} \\ &\times \operatorname{sn}\left[\eta \int_0^z \exp[\beta_2 \cos(lz') - \cos(2lz')] dz', m\right] \exp[i\phi(z, t)]. \end{aligned} \tag{15}$$

With the exact solutions in hand, we can now perform a detailed study on the condensate densities for different values of  $\beta_1$  and  $\beta_2$ , which depends upon the power of the laser beam. This comparative study suggests the relationship between the tuning of the potential and the condensate densities. Here, it is worth mentioning that one gets the localized excitation  $m = 1$ , periodic excitation  $m = 0$ , and cnoidal wave excitations  $0 < m < 1$ .

### 3. Various Trap Configurations and Matter-Wave Density

The tunable potential profiles are depicted in Figures 1 and 2 for TOL-1 and TOL-2, respectively. Figures 1a and 2a are for  $\beta_{1,2} > 0$ , whereas negative  $\beta_{1,2}$  is considered in Figures 1b and 2b. The potential profile for TOL-1 becomes nearly sinusoidal, such as an OL, for small  $\beta_1 \leq 1$  with a small amplitude. It is interesting to note that TOL-1 offers a frustrated optical lattice with a periodically laid out double-well super-lattice for larger  $\beta_1$  (Figure 1). Hence, this triple mixture of OL enables us to generate a hybrid mixture of two important lattice profiles within one. This particular merit belongs to the primality nature of TOL-1. On the other hand, the sinusoidal pattern of TOL-2 for smaller  $\beta_2$  is quite significant, unlike TOL-1 (Figure 2). In addition, it does not provide a double-well super-lattice but a wider frustrated optical lattice in comparison to TOL-1 for larger  $\beta_2$ . By changing the sign of the laser power parameters ( $\beta_1$  and  $\beta_2$ ), one can interchange the positions of the frustrated optical lattice by the double-well super-lattice for TOL-1 and frustrated depth by the main lattice depth for TOL-2. These interchanges are apparent in Figures 1 and 2. The above variations of the external trap are novel, and we would like to study the effects of trap-engineering on the condensate density. Here, for simplicity, we will study the solution with no loss/gain of the condensate atoms for which  $\xi(z, t) = 0$  and  $a(t) = \text{constant}$  in Equation (3). Initially, we discuss the TOLs in the attractive domain ( $G < 0$ ) with  $m = 1$ , and later we focus on the variations of the modulus parameter  $m$  in the TOLs for the attractive ( $G < 0$ ) domain. In the accompanying figures, for better illustration purposes, all the potentials are placed (scaled with a peak value of 0.2) alongside the normalized condensate density.

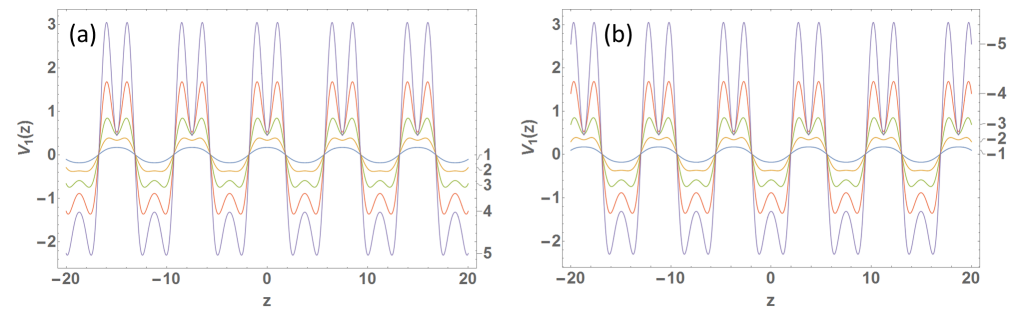


**Figure 1.** A tunable TOL-1 trap by changing  $\beta_1$ : (a) For  $\beta_1 > 0$  and  $\beta_1 = 1, 2, 3, 4, 5$  and (b) for  $\beta_1 < 0$  and  $\beta_1 = -1, -2, -3, -4, -5$ . The corresponding values of  $\beta_1$  are labeled on the right side of every figure.

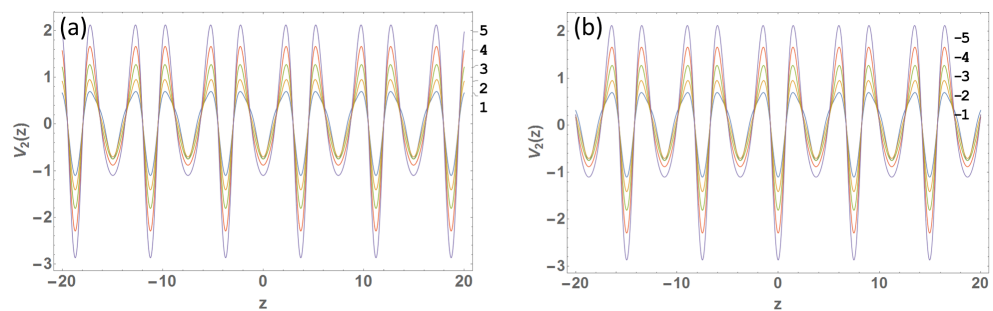


**Figure 2.** A tunable TOL-2 trap by changing  $\beta_2$ : (a) For  $\beta_2 > 0$  and  $\beta_2 = 1, 2, 3, 4, 5$  and (b) for  $\beta_2 < 0$  and  $\beta_2 = -1, -2, -3, -4, -5$ . The corresponding values of  $\beta_2$  are labeled on the right side of every figure.

### 3.1. Localized Condensate Density for TOL-1

The density profiles for  $\beta_1 > 0$  are illustrated in Figure 3 with the parameters  $G = -1$ ,  $l = 0.84$ ,  $m = 1$ ,  $a(t) = 0.1$ , and  $\eta = 0.1$ . Figure 3a approximately signifies an OL for  $\beta_1 = 1$ , where the maximum of the OL is positioned at the origin ( $z = 0$ ). When  $\beta_1$  is increased, the maxima of the optical lattice produce smaller dips (compared to the OL-minima), which are called frustrated lattice sites, whereas the minima of the OL is associated with small elevations, producing a double well in each OL-minima. Initially ( $\beta_1 = 1$ ), the condensate density is a bright solitary wave with density maxima at the minima of the lattice. Soon after the appearance of the frustrated lattice sites, the condensate gets separated and becomes more localized and starts relocating the atoms in the central frustrated site for  $\beta_1 \sim 3.25$ . A further increase in laser power will focus all the condensate atoms in the central frustrated site, manifesting an Anderson-like localization.

The effect of the double-well super-lattice is more pronounced in Figure 4, where we take  $\beta_1 < 0$ . In this domain, the center ( $z = 0$ ) contains a double-well, unlike the positive domain. For a larger magnitude of  $\beta_1$ , the barriers of the double-wells become quite significant, which effectively bifurcates the cloud at the center. We observe a complete bifurcation of the localized cloud at the center due to the broadening of the intra-well barrier for  $\beta_1 \leq -10$ .

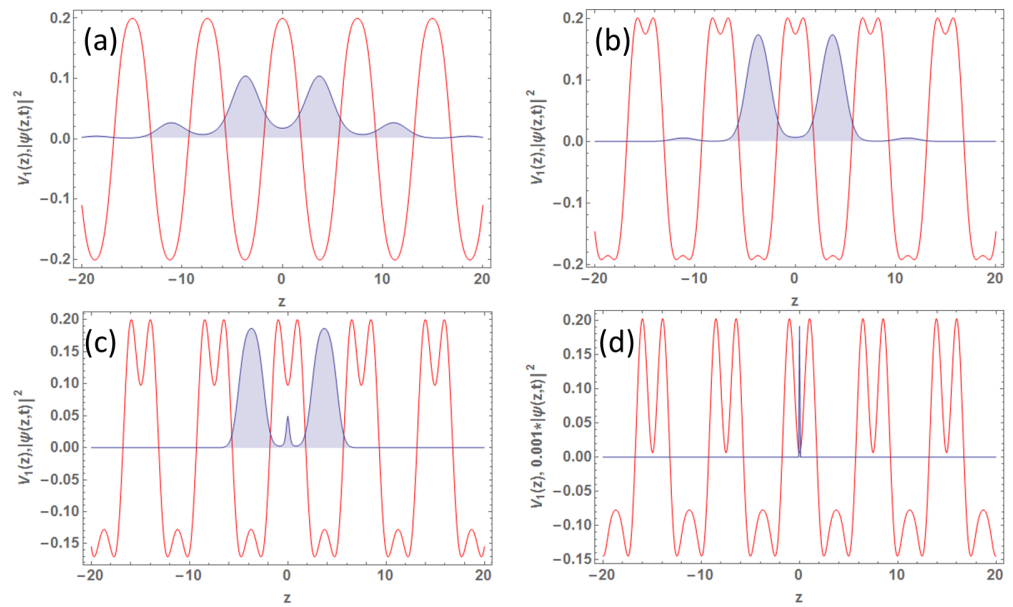


**Figure 3.** Condensate density patterns (TOL-1) for  $\beta_1 > 0$ : (a) for  $\beta_1 = 1$ , (b) for  $\beta_1 = 2$ , (c) for  $\beta_1 = 3.25$ , and (d) for  $\beta_1 = 6$ , alongside scaled potential with peak value 0.2. Other parameters are in dimensionless units:  $G = -1, l = 0.84, m = 1, a(t) = 0.1$ , and  $\eta = 0.1$ .

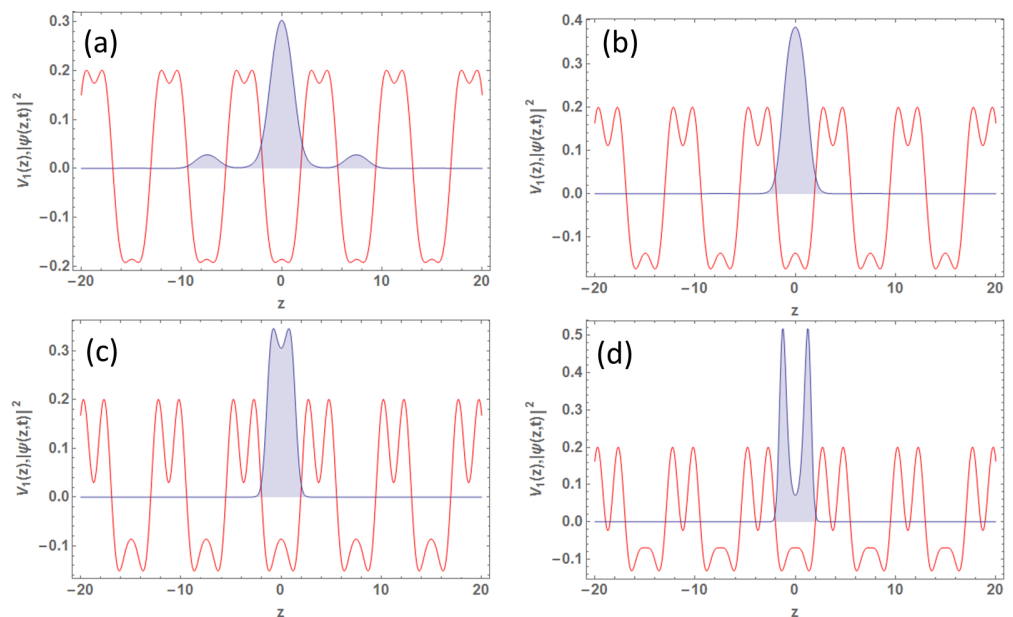


**Figure 4.** Condensate density patterns (TOL-1) for  $\beta_1 < 0$ : (a) for  $\beta_1 = -2$ , (b) for  $\beta_1 = -3$ , (c) for  $\beta_1 = -5$ , and (d) for  $\beta_1 = -8$ , alongside scaled potential with peak value 0.2. Other parameters are in dimensionless units:  $G = -1, l = 0.84, m = 1, a(t) = 0.1$ , and  $\eta = 0.1$ .

### 3.2. Localized Condensate Density for TOL-2

The density profiles for  $\beta_2 > 0$  in this case (TOL-2) is depicted in Figure 5 for  $G = -1, l = 0.84, m = 1, a(t) = 0.1$ , and  $\eta = 0.1$ . The initial density pattern is quite different from the usual bi-periodic lattice, or the density explained for TOL-1. Even for smaller laser power,  $\beta_2 = 1$ , we obtain a prominent frustrated lattice position, and accordingly, the density starts accumulating at those sites, even before reaching an overall localization of the cloud. In fact, there is competition between the two kinds of localization. Localization at frustrated sites is suppressed at the intermediate value ( $\beta_2 = 4$ ), whereas it dominates in Figure 5c,d and gets Anderson-localized. Figure 6 delineates the condensate density for  $\beta_2 < 0$ . In this case, the central site is a deeper lattice site, but not of the frustrated

kind. Hence, the finally localized cloud is not as sharp as the previous case. It is worth emphasizing that Figure 6c creates three very well-separated localized condensates. Such well-separated quantum objects can be useful for quantum information science.

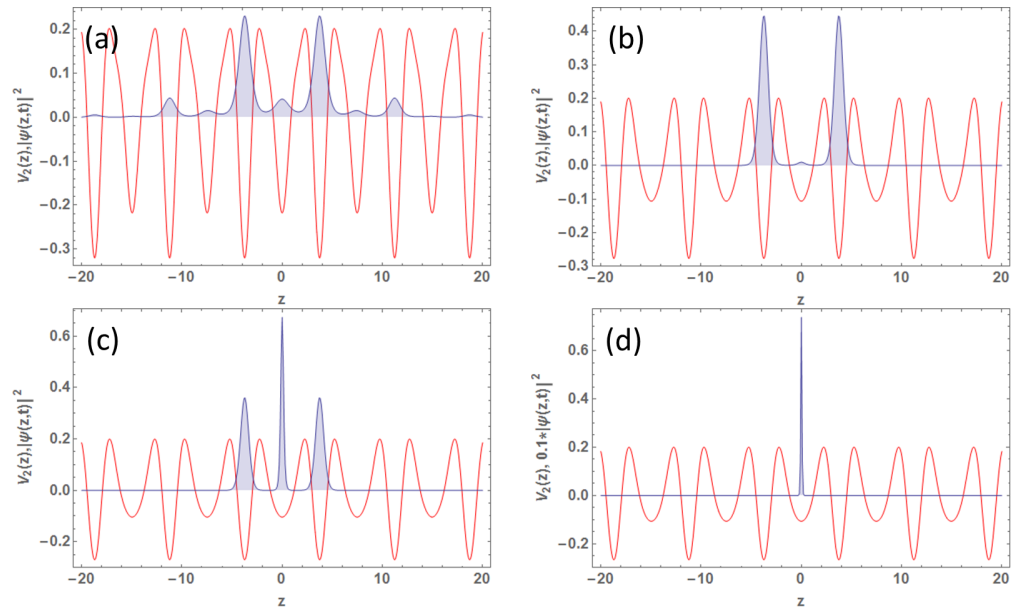


**Figure 5.** Condensate density patterns (TOL-2) for  $\beta_2 > 0$ : (a) for  $\beta_2 = 1$ , (b) for  $\beta_2 = 4$ , (c) for  $\beta_2 = 5$ , and (d) for  $\beta_2 = 6$ , alongside scaled potential with peak value 0.2. Other parameters are in dimensionless units:  $G = -1, l = 0.84, m = 1, a(t) = 0.1$ , and  $\eta = 0.1$ .

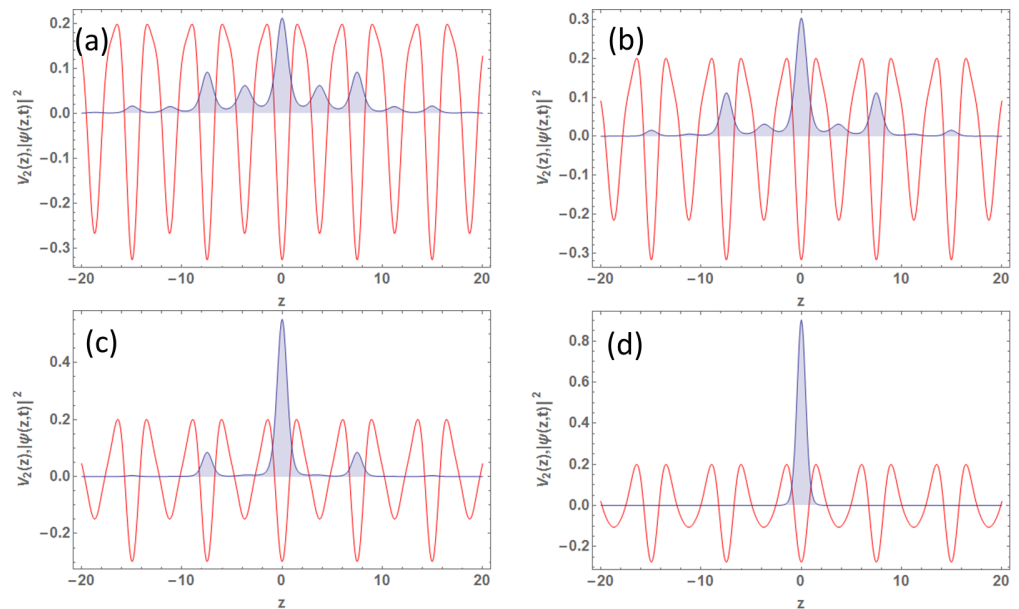


**Figure 6.** Condensate density patterns (TOL-2) for  $\beta_2 < 0$ : (a) for  $\beta_2 = -0.5$ , (b) for  $\beta_2 = -1.$ , (c) for  $\beta_2 = -2$ , and (d) for  $\beta_2 = -4$ , alongside scaled potential with peak value 0.2. Other parameters are in dimensionless units:  $G = -1, l = 0.84, m = 1, a(t) = 0.1$ , and  $\eta = 0.1$ .

### 3.3. Periodic and Cnoidal Matter-Wave Excitations

It is also intriguing to study the existence of periodic and cnoidal wave excitations, which are generally observed in nonlinear systems. A periodic density pattern in BEC is routinely studied in the context of OLs. Here, the modulus parameter controls the analytical form of a given type of excitation:  $m = 0$  provides periodic excitations, whereas  $m = 0.5$

manifests cnoidal matter-waves. In Figure 7, we have chosen a particular potential parameter for illustration ( $\beta_1 = 3.25$  for TOL-1 and  $\beta_2 = 5.0$  for TOL-2). Figure 7a–d are for TOL-1, and Figure 7e–h are for TOL-2. The potential profile and the localized condensate density are also given along with periodic and cnoidal excitations for comparison. The modulations in the fine oscillation are visible in cnoidal waves, as shown in Figure 7c,g. The periodic wave also sees the effect of the potential, which is quite patterned in Figure 7d. The studies of cnoidal waves may be useful for studying supersolidity [52].

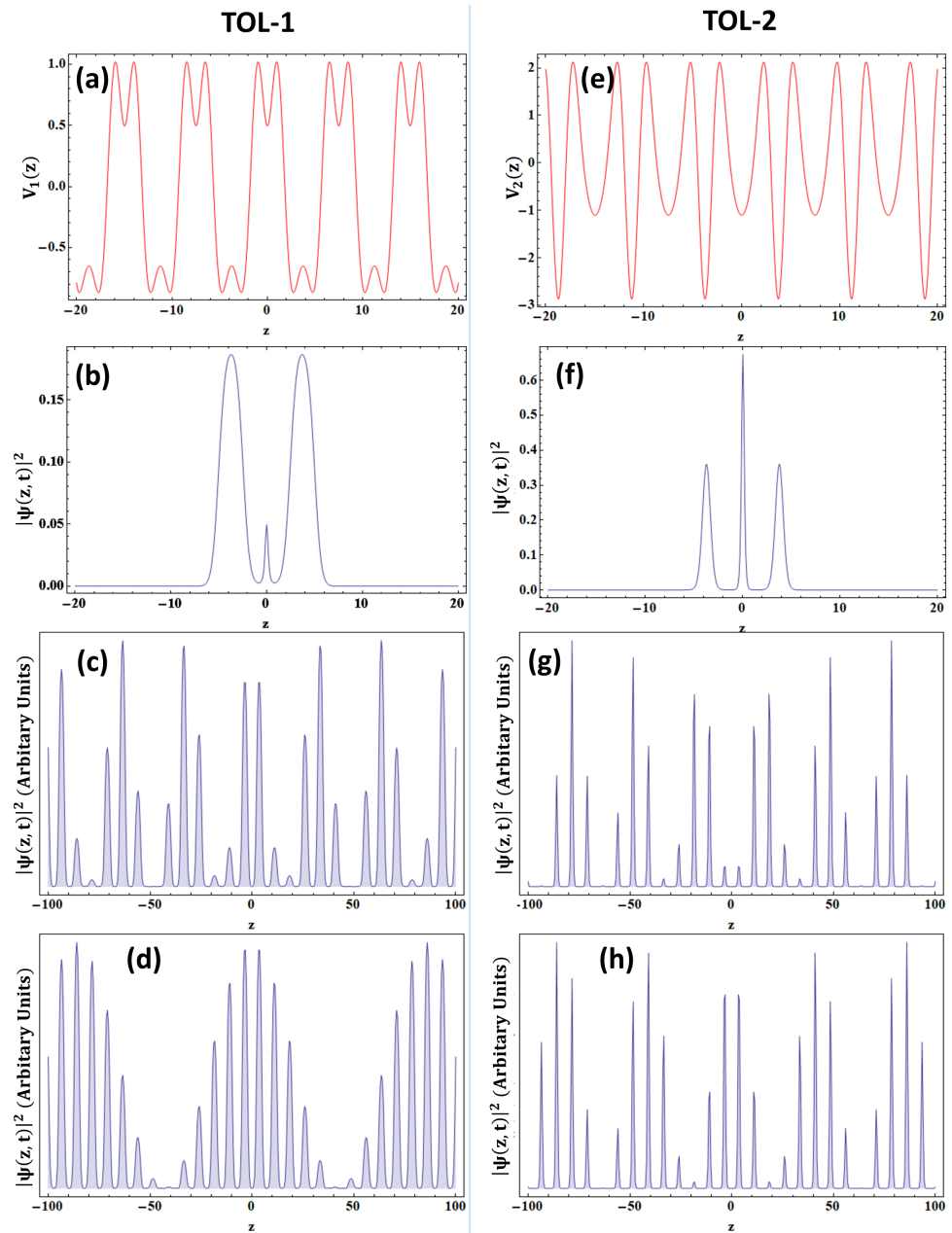


**Figure 7.** Variation of condensate density with different modulus parameters:  $\beta_1 = 3.25$  and  $\beta_2 = 5.0$  for TOL-1 and TOL-2, respectively. The represented physical quantities for TOL-1 are (a) potential profile, (b) localized condensate density for  $m = 1$ , (c) density of cnoidal matter-wave for  $m = 0.5$ , and (d) density of periodic excitation for  $m = 0$ . The same physical quantities are represented for TOL-2 in (e–h).

#### 4. Dynamical Stability and Structural Stability

To show the fruitfulness of the exact solutions as obtained from the analytical method, stability analysis needs to be performed. The stability analyses are performed by considering two situations, namely, due to the noise in the wavefunction and hence in the density (i.e., the dynamical stability); and the in-built disturbance due to the noise in the potential (i.e., the structural stability). We have analyzed both situations from the GPE using the split-step Fourier Method (SSFM) [45,53,54] for both TOL-1 and TOL-2. We add random white noise to the wavefunctions and the potentials, then allow them to evolve with time. The noisy wavefunction and the noisy potentials are given by,

$$\begin{aligned} \psi_{\text{noisy}}(z, t = 0) &= \psi(z, t = 0) + \mathcal{N}_w, \\ V_{1,\text{noisy}}(z) &= V_1(z) + \mathcal{N}_w, \\ V_{2,\text{noisy}}(z) &= V_2(z) + \mathcal{N}_w. \end{aligned} \tag{16}$$

We have performed the stability analyses for a wide range of  $\beta_1$  and  $\beta_2$  values for TOL-1 and TOL-2. However, to demonstrate the stability of the analytically derived wavefunctions, we have chosen  $\beta_1 = 2$  and  $\beta_2 = 2$ . The amplitude of noise,  $\mathcal{N}_w$  is varied from 0% to 5% of the maximum value of the amplitude of the initial unperturbed wavefunction. While studying the dynamical stability, we first evolved the wavefunction without noise and the wavefunction with noise. The corresponding condensate density is compared by finding the deviation, i.e.,  $D_W = |\psi_{\text{wn}}(z, t)|^2 - |\psi_{\text{wn}}(z, t = 0)|^2$ , where  $\psi_{\text{wn}}(z, t)$  stands for noisy wavefunction. We follow the same procedure for finding the deviation for structural stability where the noise is added to the potential:  $D_P = |\psi_{\text{pn}}(z, t)|^2 - |\psi_{\text{pn}}(z, t = 0)|^2$ , where  $\psi_{\text{pn}}(z, t)$  stands for the wavefunction with noise added to the potential. We have simulated the evolutions for 10000 time iterations with temporal and spatial step sizes,  $dt = 0.224 \mu\text{s}$  and  $dz = 0.277 \mu\text{m}$ . In Figure 8a,b, we depict the potentials (TOL-1 and TOL-2) without noise, condensate densities without noise and the deviations due to dynamical stability and structural stability for both cases. To enable us to illustrate all of them in one plot, the potentials are scaled by 0.2, and the deviations ( $D_W$  (in  $*$ ) and  $D_P$  (in  $\oplus$ )) are placed at  $(0, 0.28)$  and  $(0, -0.08)$ , respectively, where the magnitude of the deviation is represented by their amplitude variations.

For Figure 8a,b the deviation values  $D_W$  (in  $*$ ) and  $D_P$  (in  $\oplus$ ) are shown in the figures with shifted coordinates at  $(0, 0.28)$  (upper plots) and  $(0, -0.08)$  (lower plots), respectively, with the potential being scaled with 0.2. We obtain attractive results where the solutions are extremely stable for structural noise incorporation, and the maximum deviation becomes only 1% for both the potential profiles (TOL-1 and TOL-2). The dynamical stability also suggests considerably stable solutions, having a maximum deviation below 5%. Hence, both the proposed triple optical lattices offer experimentally feasible platforms to study various solitary waves in BEC.

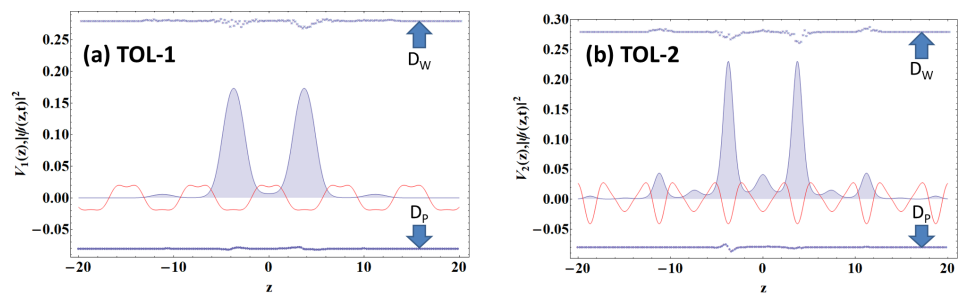


**Figure 8.** Numerical stability analysis for : (a) TOL-1 with  $\beta_1 = 2$  and (b) TOL-2 with  $\beta_2 = 2$ . In both plots, the condensate densities are presented as filled plots, and the potential profiles are placed together by scaling with 0.2. The deviation values for dynamical stability,  $D_W$  and for structural stability,  $D_P$ , are shown at the coordinates  $(0, 0.28)$  (upper plots) and  $(0, -0.08)$  (lower plots), respectively, for both (a) and (b).

## 5. Conclusions

Even and odd combinations of OLs physically provide distinct environments for the condensate. We have introduced two varieties of odd numbered optical lattice-combination for BEC, which are not given due emphasize in the theory-literature, are addressed with triple optical lattices which manifest hybrid trap with a highly stable condensate compared to other traps. In addition to the localized excitation, periodic and cnoidal waves are also studied. Anderson localization, bifurcation of condensate at the center and a competition of different localizations upon trap engineering in these TOLs are reported. These triple mixtures of optical lattices impart better tunability on the condensate profile, which has made this system a true quantum simulator. For checking the utility of the results for experiments, we have performed dynamical and structural stability analyses. The solutions have come out as extremely stable for structural noise incorporation, having deviation below 1% for both the potential profiles. The dynamical stability also suggests considerably stable solutions, having deviation below 5%. Hence, both the proposed triple optical lattices offer favorable platforms to study various solitary waves in BEC and possible technological implications.

**Author Contributions:** Conceptualization, U.R.; formal analysis, P.B., B.H. and S.R.; investigation, P.B., B.H., S.R. and U.R.; methodology, P.B. and U.R.; software, B.H.; validation, S.R. and U.R.; visualization, P.B. and S.R.; writing—original draft preparation, P.B. and B.H.; writing—review and editing, S.R. and U.R.; supervision, U.R. All authors have read and agreed to the published version of the manuscript.

**Funding:** This research received no external funding.

**Institutional Review Board Statement:** Not applicable.

**Informed Consent Statement:** Not applicable.

**Data Availability Statement:** Not applicable.

**Acknowledgments:** P.B. is thankful to the Prime Minister Research Fellowship (PMRF), Government of India, for the financial support throughout the research.

**Conflicts of Interest:** The authors declare no conflict of interest.

## References

1. Pethick, C.J.; Smith, H. *Bose–Einstein Condensation in Dilute Gases*; Cambridge University Press: Cambridge, UK, 2008.
2. Pitaevskii, L.; Stringari, S. *Bose–Einstein Condensation*; Oxford University Press: Oxford, UK, 2003.
3. Nath, A.; Roy, U. A unified model for an external trap in a cigar-shaped Bose–Einstein condensate. *J. Phys. A Math. Theor.* **2014**, *47*, 415301. [[CrossRef](#)]
4. Salasnich, L.; Adhikari, S.K. Dimensional reduction and localization of a Bose-Einstein condensate in a quasi-1D bichromatic optical lattice. *Acta Phys. Pol. A* **2015**, *128*, 979. [[CrossRef](#)]
5. Khaykovich, L.; Schreck, F.; Ferrari, G.; Bourdel, T.; Cubizolles, J.; Carr, L.D.; Castin, Y.; Salomon, C. Formation of a matter-wave bright soliton. *Science* **2002**, *296*, 1290–1293. [[CrossRef](#)] [[PubMed](#)]
6. Schulte, T.; Drenkelforth, S.; Kruse, J.; Ertmer, W.; Arlt, J.; Sacha, K.; Zakrzewski, J.; Lewenstein, M. Routes towards Anderson-like localization of Bose-Einstein condensates in disordered optical lattices. *Phys. Rev. Lett.* **2005**, *95*, 170411. [[CrossRef](#)] [[PubMed](#)]
7. Billy, J.; Josse, V.; Zuo, Z.; Bernard, A.; Hambrecht, B.; Lugan, P.; Clément, D.; Sanchez-Palencia, L.; Bouyer, P.; Aspect, A. Direct observation of Anderson localization of matter waves in a controlled disorder. *Nature* **2008**, *453*, 891–894. [[CrossRef](#)] [[PubMed](#)]
8. Nath, A.; Bera, J.; Ghosh, S.; Roy, U. exact Analytical Model for Bose-einstein condensate at negative temperature. *Sci. Rep.* **2020**, *10*, 9016. [[CrossRef](#)]
9. Kundu, N.; Nath, A.; Bera, J.; Ghosh, S.; Roy, U. Synergy between the Negative Absolute Temperature and the External Trap for a Bose-Einstein Condensate under Optical Lattices. *Phys. Lett. A* **2022**, *427*, 127922. [[CrossRef](#)]
10. Yamamoto, D.; Fukuhara, T.; Danshita, I. Frustrated quantum magnetism with Bose gases in triangular optical lattices at negative absolute temperatures. *Commun. Phys.* **2020**, *3*, 56. [[CrossRef](#)]
11. D’Errico, C.; Burchianti, A.; Prevedelli, M.; Salasnich, L.; Ancilotto, F.; Modugno, M.; Minardi, F.; Fort, C. Observation of quantum droplets in a heteronuclear bosonic mixture. *Phys. Rev. Res.* **2019**, *1*, 033155. [[CrossRef](#)]
12. Perali, A.; Pieri, P.; Pisani, L.; Strinati, G.C. BCS-BEC crossover at finite temperature for superfluid trapped Fermi atoms. *Phys. Rev. Lett.* **2004**, *92*, 220404. [[CrossRef](#)]

13. Chen, Q.; Stajic, J.; Tan, S.; Levin, K. BCS–BEC crossover: From high temperature superconductors to ultracold superfluids. *Phys. Rep.* **2005**, *412*, 1–88. [[CrossRef](#)]
14. Zwerger, W. *The BCS-BEC Crossover and the Unitary Fermi Gas*; Springer: Berlin/Heidelberg, Germany, 2011; Volume 836.
15. Cronin, A.D.; Schmiedmayer, J.; Pritchard, D.E. Optics and interferometry with atoms and molecules. *Rev. Mod. Phys.* **2009**, *81*, 1051. [[CrossRef](#)]
16. Billam, T.; Cornish, S.; Gardiner, S. Realizing bright-matter-wave-soliton collisions with controlled relative phase. *Phys. Rev. A* **2011**, *83*, 041602. [[CrossRef](#)]
17. Struck, J.; Ölschläger, C.; Le Targat, R.; Soltan-Panahi, P.; Eckardt, A.; Lewenstein, M.; Windpassinger, P.; Sengstock, K. Quantum simulation of frustrated classical magnetism in triangular optical lattices. *Science* **2011**, *333*, 996–999. [[CrossRef](#)]
18. Balents, L. Spin liquids in frustrated magnets. *Nature* **2010**, *464*, 199–208. [[CrossRef](#)]
19. Yan, S.; Huse, D.A.; White, S.R. Spin-liquid ground state of the  $S = 1/2$  Kagome Heisenberg antiferromagnet. *Science* **2011**, *332*, 1173–1176. [[CrossRef](#)]
20. Qiu, X.; Zou, J.; Qi, X.; Li, X. Precise programmable quantum simulations with optical lattices. *Npj Quantum Inf.* **2020**, *6*, 87. [[CrossRef](#)]
21. Windpassinger, P.; Sengstock, K. Engineering novel optical lattices. *Rep. Prog. Phys.* **2013**, *76*, 086401. [[CrossRef](#)]
22. Kundu, N.; Ghosh, S.; Roy, U. Quantum Simulation of Rogue Waves in Bose-Einstein Condensate: An Exact Analytical Method. *Phys. Lett. A* **2022**, 128335. [[CrossRef](#)]
23. Argüello-Luengo, J.; González-Tudela, A.; Shi, T.; Zoller, P.; Cirac, J.I. Quantum simulation of two-dimensional quantum chemistry in optical lattices. *Phys. Rev. Res.* **2020**, *2*, 042013. [[CrossRef](#)]
24. Arlinghaus, S.; Holthaus, M. Controlled wave-packet manipulation with driven optical lattices. *Phys. Rev. A* **2011**, *84*, 063617. [[CrossRef](#)]
25. Covey, J.P.; Moses, S.A.; Gärttner, M.; Safavi-Naini, A.; Mieczkowski, M.T.; Fu, Z.; Schachenmayer, J.; Julienne, P.S.; Rey, A.M.; Jin, D.S.; et al. Doublon dynamics and polar molecule production in an optical lattice. *Nat. Commun* **2016**, *7*, 11279. [[CrossRef](#)]
26. Casert, C.; Mills, K.; Vieijra, T.; Ryckebusch, J.; Tamblyn, I. Optical lattice experiments at unobserved conditions with generative adversarial deep learning. *Phys. Rev. Res.* **2021**, *3*, 033267. [[CrossRef](#)]
27. Homid, A.; Abdel-Aty, M.; Qasymeh, M.; Eleuch, H. Efficient quantum gates and algorithms in an engineered optical lattice. *Sci. Rep.* **2021**, *11*, 15402. [[CrossRef](#)] [[PubMed](#)]
28. Katori, H. Optical lattice clocks and quantum metrology. *Nat. Photon.* **2011**, *5*, 203–210. [[CrossRef](#)]
29. Ghosh, S.; Bera, J.; Panigrahi, P.K.; Roy, U. Sub-fourier quantum metrology through bright solitary trains in Bose–Einstein condensate. *Int. J. Quantum Inf.* **2019**, *17*, 1950019. [[CrossRef](#)]
30. Cameron, A.R.; Cheng, S.W.; Schwarz, S.; Kapahi, C.; Sarenac, D.; Grabowecy, M.; Cory, D.G.; Jennewein, T.; Pushin, D.A.; Resch, K.J. Remote state preparation of single-photon orbital-angular-momentum lattices. *Phys. Rev. A* **2021**, *104*, L051701. [[CrossRef](#)]
31. Simon, D.S. Quantum sensors: Improved optical measurement via specialized quantum states. *J. Sens.* **2016**, *2016*, 6051286. [[CrossRef](#)]
32. Yang, B.; Sun, H.; Huang, C.J.; Wang, H.Y.; Deng, Y.; Dai, H.N.; Yuan, Z.S.; Pan, J.W. Cooling and entangling ultracold atoms in optical lattices. *Science* **2020**, *369*, 550–553. [[CrossRef](#)]
33. Howard, L.; Weinhold, T.; Shahandeh, F.; Combes, J.; Vanner, M.; White, A.; Ringbauer, M. Quantum hypercube states. *Phys. Rev. Lett.* **2019**, *123*, 020402. [[CrossRef](#)]
34. Shukla, N.; Akhtar, N.; Sanders, B.C. Quantum tetrachotomous states: Superposition of four coherent states on a line in phase space. *Phys. Rev. A* **2019**, *99*, 063813. [[CrossRef](#)]
35. Shukla, N.; Nimmrichter, S.; Sanders, B.C. Squeezed comb states. *Phys. Rev. A* **2021**, *103*, 012408. [[CrossRef](#)]
36. Roy, U.; Atre, R.; Sudheesh, C.; Kumar, C.N.; Panigrahi, P.K. Complex solitons in Bose–Einstein condensates with two- and three-body interactions. *J. Phys. B At. Mol. Opt.* **2010**, *43*, 025003. [[CrossRef](#)]
37. Serkin, V.N.; Hasegawa, A. Novel soliton solutions of the nonlinear Schrödinger equation model. *Phys. Rev. Lett.* **2000**, *85*, 4502. [[CrossRef](#)]
38. Liang, Z.; Zhang, Z.; Liu, W. Dynamics of a bright soliton in Bose-Einstein condensates with time-dependent atomic scattering length in an expulsive parabolic potential. *Phys. Rev. Lett.* **2005**, *94*, 050402.
39. Belmonte-Beitia, J.; Pérez-García, V.M.; Vekslerchik, V.; Torres, P.J. Lie symmetries and solitons in nonlinear systems with spatially inhomogeneous nonlinearities. *Phys. Rev. Lett.* **2007**, *98*, 064102. [[CrossRef](#)]
40. Yan, Z.; Jiang, D. Matter-wave solutions in Bose-Einstein condensates with harmonic and Gaussian potentials. *Phys. Rev. E* **2012**, *85*, 056608. [[CrossRef](#)]
41. Bludov, Y.V.; Yan, Z.; Konotop, V. Dynamics of inhomogeneous condensates in contact with a surface. *Phys. Rev. A* **2010**, *81*, 063610. [[CrossRef](#)]
42. Bronski, J.C.; Carr, L.D.; Deconinck, B.; Kutz, J.N. Bose-Einstein condensates in standing waves: The cubic nonlinear Schrödinger equation with a periodic potential. *Phys. Rev. Lett.* **2001**, *86*, 1402. [[CrossRef](#)]
43. Adhikari, S.; Salasnich, L. Localization of a Bose-Einstein condensate in a bichromatic optical lattice. *Phys. Rev. A* **2009**, *80*, 023606. [[CrossRef](#)]
44. Nath, A.; Roy, U. Bose–Einstein condensate in a bichromatic optical lattice: An exact analytical model. *Laser Phys. Lett.* **2014**, *11*, 115501. [[CrossRef](#)]

45. Halder, B.; Ghosh, S.; Basu, P.; Bera, J.; Malomed, B.; Roy, U. Exact Solutions for Solitary Waves in a Bose-Einstein Condensate under the Action of a Four-Color Optical Lattice. *Symmetry* **2021**, *14*, 49. [[CrossRef](#)]
46. Dell'Anna, L.; Mazzarella, G.; Penna, V.; Salasnich, L. Entanglement entropy and macroscopic quantum states with dipolar bosons in a triple-well potential. *Phys. Rev. A* **2013**, *87*, 053620. [[CrossRef](#)]
47. Witthaut, D.; Trimborn, F.; Hennig, H.; Kordas, G.; Geisel, T.; Wimberger, S. Beyond mean-field dynamics in open Bose-Hubbard chains. *Phys. Rev. A* **2011**, *83*, 063608. [[CrossRef](#)]
48. Dutta, S.; Tsatsos, M.C.; Basu, S.; Lode, A.U. Management of the correlations of Ultracold Bosons in triple wells. *New J. Phys.* **2019**, *21*, 053044. [[CrossRef](#)]
49. Kengne, E.; Liu, W.M.; Malomed, B.A. Spatiotemporal engineering of matter-wave solitons in Bose–Einstein condensates. *Phys. Rep.* **2021**, *899*, 1–62. [[CrossRef](#)]
50. Salasnich, L.; Parola, A.; Reatto, L. Effective wave equations for the dynamics of cigar-shaped and disk-shaped Bose condensates. *Phys. Rev. A* **2002**, *65*, 043614. [[CrossRef](#)]
51. Abramowitz, M.; Stegun, I.A. *Handbook of Mathematical Functions with Formulas, Graphs, and Mathematical Tables*; US Government Printing Office; Washington, DC, USA, 1964; Volume 55,
52. Martone, G.I.; Recati, A.; Pavloff, N. Supersolidity of cnoidal waves in an ultracold Bose gas. *Phys. Rev. Res.* **2021**, *3*, 013143. [[CrossRef](#)]
53. Nath, A.; Bera, J.; Ghosh, S.; Panigrahi, P.K.; Roy, U. Soliton dynamics for an ingenious trap combination in a Bose-Einstein condensate. *Eur. Phys. J. D* **2020**, *74*, 27. [[CrossRef](#)]
54. Bera, J.; Ghosh, S.; Salasnich, L.; Roy, U. Matter-wave fractional revivals in a ring waveguide. *Phys. Rev. A* **2020**, *102*, 063323. [[CrossRef](#)]